Theory of dielectric nanofilms in strong ultrafast optical fields

Vadym Apalkov and Mark I. Stockman

Phys. Rev. B **86**, 165118 — Published 11 October 2012

DOI: 10.1103/PhysRevB.86.165118

Theory of dielectric nanofilms in strong ultrafast optical fields

Vadym Apalkov and Mark I. Stockman
Department of Physics and Astronomy, Georgia State University, Atlanta, Georgia 30303, USA

We theoretically predict that a dielectric nanofilm subjected to a normally-incident strong but ultrashort (a few optical oscillations) laser pulse exhibits deeply nonlinear (non-perturbative) optical responses which are essentially reversible and driven by the instantaneous optical field. Among them is a high optical polarization and a significant population of the conduction band, which develop at the peak of the pulse and almost disappear after its end. There is also a correspondingly large increase of the pulse reflectivity. These phenomena are related to Wannier-Stark localization and anticrossings between the Wannier-Stark ladders originating from the valence and conduction bands leading to optical "softening" of the dielectric. Theory is developed by solving self-consistently the Maxwell equations and the time-dependent Schrödinger equation. The results point out to a fundamental possibility of optical-field effect devices with the bandwidth on the order of optical frequency.

PACS numbers:

I. INTRODUCTION

Experimental availability of intense ultrashort (a few femtosecond-long) optical pulses with just a few oscillations of optical field opens up unique possibilities of optical control of the electric and optical properties of dielectric materials within femtosecond time scale[1,2]. The electric field in such intense optical pulses is comparable to the internal fields acting on valence electrons in atoms and solids and is on the order of a few V/Å[2,3]. Interaction of the electrons of a solid with such strong fields has long been the subject of intensive research[4–8]. A strong-field optical pulse induces deep changes of the system, which can be reversible for a short enough pulse[3,9–13].

For semiconductors and their heterostructures, the optical field causes decrease of the bandgap between the valence and conduction band known as Franz-Keldysh effect[14,15] and quantum-confined Stark effect[16,17], respectively. For conjugated molecules, which are organic semiconductors, it has been predicted that the Stark effect decreases the gap between the occupied and unoccupied molecular orbits leading to absorption of the initially non-resonant pulses and electrical currents due to the $\omega - 2\omega$ interference[18].

A dielectric subjected to a weak optical field reacts to its change instantly (adiabatically) as long as the laser frequency ω_0 is small enough, $\omega_0 \ll \Delta_g/\hbar$, where Δ_g is the gap between the valence band (VB) and conduction band (CB); e.g, for silica $\Delta_g \approx 9$ eV. This adiabaticity implies that the light-matter interaction is fully reversible: after the pulse end, the system returns to its ground state, the residual excited-band population is small, and so is the residual interband polarization. This is expected for wide-bandgap dielectrics.

When the pulse field F increases, approaching the critical field strength F_{crit}, which induces a change in electron potential energy by Δ_g over the lattice period $a \sim 5$ Å, the adiabatic band gap decreases and completely collapses, where

$$F_{crit} = \frac{\Delta_g}{|e|a} \sim 2\frac{\mathrm{V}}{\mathrm{Å}} , \tag{1}$$

and e is electron charge.

Previously, theoretical analysis of interaction of a intense optical pulse with dielectric media was mainly restricted to relatively long pulses with duration $\gtrsim 100$ fs. For such pulses, the electron dynamics in the time-dependent field of the pulse be described in terms of the density matrix whose evolution is determined by rate equations with phenomenological relaxation and generation times[19–23]. In this description, the effect of the pulse electric field is restricted to generation of an electron-hole plasma through multiphoton or collisional ionization processes. Such rates as functions of the instantaneous electric field are usually introduced into the model phenomenologically.

Another theoretical approach to interaction of ultrashort optical pulse with semiconductor and dielectric media was introduced in Refs. 24–26. In these publications, a coupled system of Maxwell equations and time-dependent density-functional theory equations is solved numerically for diamond or silicon. In Ref. 26, the frequency of the pulse is close to the interband gap, i.e., the system is close to the resonance conditions. Therefore, although the duration of the pulse is small, ~ 10 fs, the dielectric system experiences a non-adiabatic dynamics with high residual excitation and a strong increase of the pulse reflectance.

In the present article, we consider an extremely intense and ultrashort pulse with duration of a several femtoseconds, and the dielectric system far away from the resonant conditions. Specifically, we consider silica with bandgap $\Delta_g \approx 9$ eV and pulse carrier frequency $\hbar\omega_0 = 1.5$ eV. With relaxation time ~ 20 fs, the electron dynamics for such an ultrashort pulse is expected to be field-driven and coherent (Hamiltonian), which can be described in terms of wave functions[11,13]. We introduce a coupled system of Maxwell equations and the time-

dependent Schrödinger equation, and solve it numerically. The Hamiltonian of the dielectric system is of the nearest neighbor tight-binding type with the parameters chosen to reproduce the band structure of silica. Within this approach, the electric field of the pulse couples the states of the VB and the CB of the dielectric. Inherent in this system, electrons are dynamically transferred to the CB without any assumptions about the generation rate. We apply this approach to a nanofilm of silica with a thickness of ≤ 150 nm.

Under such conditions, the underlying electronic dynamics is characterized by a strong localization of the Wannier-Stark (WS) states[7,27]. These states originating from a given band are separated by the Bloch oscillation frequency[28], which significantly exceeds ω_0. Thus the electron dynamics is mostly adiabatic except for anticrossings of the Wannier-Stark levels originating from different bands. At those anticrossings, rich dynamics appears, which generally is a superposition of both diabatic and adiabatic processes. This leads to "softening" of the system: enhanced optical responses of the dielectric, in particular strong polarization and reflection of the pulse, which are deeply nonlinear (non-perturbative) phenomena. For the strong ultrafast fields that are still below the threshold of the dielectric breakdown, the dynamics is reversible: the electron population of the CB left after the pulse end is very low in contrast to a relatively high CB population during the pulse.

With respect to the previous prediction of the adiabatic metallization of dielectric nanofilms[11,13], a significant difference is that the present processes are too fast to be predominantly adiabatic. Also of fundamental importance is that in the present work the pulse field is parallel to the surface while in Refs. 11,13 it is normal to the surface causing appearance of the so-called quantum bouncer states playing an important role.

The paper is organized as the following. In Sec. II, we derive the main system of equations, which includes the Maxwell equations and the Schrödinger equation. In Sec. III, we introduce the Wannier-Stark states of CB and VB, and coupled adiabatic states of electron system in the external electric field. We discuss formation of the Wannier-Stark states of a single band for time-dependent electric field of the excitation near-infrared (NIR) pulse. In Sec. IV, we present the results of the calculations and discuss physical interpretation of these results. In Sec. V we present the concluding discussion of the obtained results.

II. MODEL AND MAIN EQUATIONS

A. Propagation of optical pulse

We study propagation of an optical pulse using a coupled system of equations, consisting of Maxwell equations, which describe the propagation of the pulse in a system with a known polarization, and the Schrödinger equations, which determine electron dynamics and the polarization of the electron system. The Maxwell equations are written down in the following form

$$\nabla \cdot \mathbf{D} = 0 \tag{2}$$

$$\nabla \cdot \mathbf{B} = 0 \tag{3}$$

$$\nabla \times \mathbf{F} = -\frac{1}{c}\frac{\partial \mathbf{B}}{\partial t} \tag{4}$$

$$\nabla \times \mathbf{B} = \frac{1}{c}\frac{\partial \mathbf{F}}{\partial t} + \frac{4\pi}{c}\frac{\partial \mathbf{P}}{\partial t} \tag{5}$$

where $\mathbf{B}$ is magnetic field, $\mathbf{F}$ is electric field, and $\mathbf{D} = \mathbf{F} + 4\pi\mathbf{P}$ is the electric displacement field.

The polarization $\mathbf{P}$ of the dielectric medium is determined by electron dynamics. This polarization, which is calculated in the next section, depends on the electric field of the pulse in a strongly nonlinear manner due to strong mixing of CB and VB states in a high electric field.

Solution of the Maxwell equations determines the propagation of the optical laser pulse and the fields outside and inside the dielectric. The way we solve them takes into account the boundary conditions at the surface of dielectric film automatically. We assume that the optical pulse propagates along the positive direction of the z-axis i.e., it is incident normally on the dielectric film. In this case, all variables in the Maxwell equations depend on z only, and the problem becomes effectively one-dimensional.

We solve the Maxwell equations numerically by the finite difference time domain (FDTD) method[29,30] for a finite size system with the absorbing boundary conditions. The size of the computational space in the z direction is 6000 nm with the coordinates of the boundaries $z_1 = -3000$ nm and $z_2 = 3000$ nm. The dielectric film is placed at the mid plane of the system, i.e, it is centered at $z = 0$. The optical pulse is generated at the left boundary and propagates along the positive direction of the z axis with the polarization of the electric field along the x axis. We assume that the pulse has the following shape,

$$F_x(t) = F_0 e^{-(\Gamma_V t)^2} \cos(\omega_0 t), \tag{6}$$

where F_0 is the amplitude of the pulse, which is related to its power, $\mathcal{P}$, thorough the relation $\mathcal{P} = cF_0^2/4\pi$; $\tau_p = 1/\Gamma_V$ is the duration of the pulse, ω_0 is the carrier frequency of the pulse. Below we assume that the frequency of the pulse is in the near-infrared (NIR) range, $\hbar\omega_0 = 1.5$ eV, and the duration of the pulse is $\tau_p = 4$ fs.

In FDTD solutions of the Maxwell equations, we choose the spatial step to be 1 nm, while the time step is 0.7 attoseconds (1 as=10^{-18} s). These values provide convergence for both the Maxwell equations and the Schrödinger equation – see Sec. IIB.

B. Electron dynamics

We capitalize on the fact that in our case the pulse length $\tau_p = 4$ fs is very short. In fact, it is much shorter

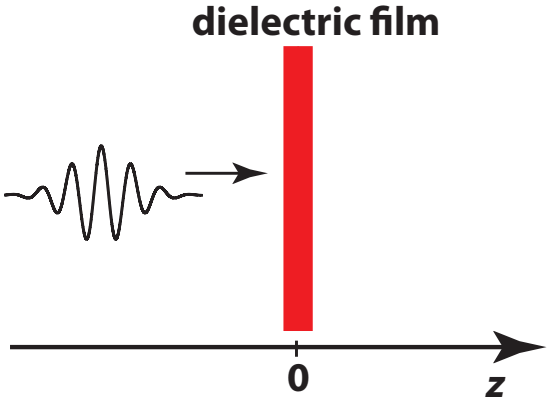

FIG. 1: Schematic illustration of the pulse normally incident on the dielectric film. The pulse is propagating in the positive direction of axis z. The dielectric film of a finite thickness, $d < 150$ nm, is placed at $z = 0$. The size of the system in z direction is 6000 nm.

than typical time of the electron-electron Coulomb interaction τ_e. For instance, in such a good metal as silver, $\tau_e \approx 20$ fs – see, e.g., Ref. 31, i.e., $\tau_p \ll \tau_e$. Hence, during the pulse duration the electron-electron collisions do not have time to produce a significant effect on the electron dynamics. Correspondingly, we will neglect the Coulomb interaction and describe the light-matter interaction by one-particle Schrödinger equation.

The electron dynamics in a periodic lattice potential in the presence of an external electric field F_x is described by the Hamiltonian:

$$\mathcal{H} = \frac{\mathbf{p}^2}{2m} + V(\mathbf{r}) + eF_x(z,t)x, \tag{7}$$

where $V(\mathbf{r})$ is the periodic crystal potential, m is the electron mass, and e is elementary charge. The electric field, $F_x(z,t)$, which is calculated from the Maxwell equations (2)-(5), depends on the z coordinate and time t.

Without an external electric field, the periodic potential, $V(\mathbf{r})$, produces the standard band structure of a solid with conduction and valence bands. The external electric field results in time-dependent coupling between different bands. For $F_x(z,t)$ periodic in t, which our field is not, such a coupling would be described by quasienergies.

Below we carry out our analysis for a multi-band system that includes both the conduction and valence bands. We denote the numbers of the conduction and valence bands as N_c and N_v, respectively, where the total number of bands is $N_{\rm bands} = N_c + N_v$. The bands are labeled by index $\alpha = 1, \ldots, N_{\rm bands}$.

For simplicity, we also assume that the periodic potential is separable in the x, y, and z-directions. Then for each value of the z coordinate, the electron dynamics in the x direction, i.e., in the direction of external electric field, becomes decoupled from the motion along the z and y directions. Correspondingly, in the y and z directions the potential is periodic with period a. In the x direction, the potential is aperiodic: it is a superposition of the periodic crystal potential and the external potential of the uniform electric field, $eF_x(z,t)x$, depending on the z coordinate as a parameter and on time t.

In the absence of an external field, the eigenfunctions of Hamiltonian (7) in the x direction are Bloch functions, $\psi_{\alpha k}(x)$, which are labeled by wave vector k, $-\pi/a < k \leq \pi/a$, and have the following form

$$\psi_{\alpha k}(x) = \frac{1}{2\pi} e^{ikx} u_{\alpha k}(x) \ , \tag{8}$$

where $u_{\alpha k}(x+a) = u_{\alpha k}(z)$ are periodic Bloch unit-cell functions. In the zero external field, the Bloch functions diagonalize the Hamiltonian (7) yielding energy dispersion relation $E_\alpha(k)$ for a band α.

We use an approximation of the tight-binding model[32,33] for dispersion relations of the conduction and valence bands,

$$E_\alpha(k) = \varepsilon_\alpha + \frac{\Delta_\alpha}{2}\cos(ka), \tag{9}$$

where Δ_α is the width of band α and ε_α is the band offset, which is the midpoint of the band α.

The external electric field, $F_x(z,t)$, introduces coupling of states of different bands and also causes time dependence of the electronic wave functions. Using the Bloch functions as the basis, we can express the general solution of the time-dependent Schrödinger equation in the following form

$$\Psi(x,z,t) = \sum_{\alpha=1}^{N_{\rm bands}} \sqrt{\frac{a}{2\pi}} \int_{-\pi/a}^{\pi/a} dk \ \phi_\alpha(k,z,t)\psi_{\alpha k}(x). \tag{10}$$

Here the dependence of the wave function, $\Psi(x,z,t)$, on coordinate z is due to electromagnetic wave propagation expressed as the dependence $F_x(z,t)$ on coordinate z. Substituting expression (10) of the wave function into the Schrödinger equation $i\hbar\partial\Psi/\partial t = \mathcal{H}\Psi$, we obtain equations[34,35] on expansion coefficients $\phi_\alpha(k,z,t)$

$$i\hbar\frac{d\phi_\alpha(k,z,t)}{dt} = \left[E_\alpha(k) + ieF_x(z,t)\frac{d}{dk}\right]\phi_\alpha(k,t) + F_x(z,t)\sum_{\alpha'} Z_{\alpha\alpha'}\phi_{\alpha'}(k,z,t), \tag{11}$$

where

$$Z_{\alpha\alpha'} = \frac{e}{a}\int_{-a}^{a} dz \ u_{\alpha k}(z)^* i\frac{\partial}{\partial k}u_{\alpha' k}(z) \tag{12}$$

are parameters of the model, which are the dipole matrix elements between the unit-cell Bloch functions of bands α and α'.

For a single band and in a constant electric field F_x, solutions of Eq. (11) are Wannier-Stark states[27,28], which

are parametrized by an integer quantum number l and have wave functions[35]

$$\tilde{\phi}_{\alpha l}(k) = e^{i[lak+\gamma_\alpha \sin(ka)]}, \tag{13}$$

where $\gamma_\alpha = \Delta_\alpha/(2eaF_x)$. In the coordinate representation,

$$\tilde{\phi}_{\alpha l}(x) = J_{l-x/a}(\gamma_\alpha) \ , \tag{14}$$

where $J_n(x)$ is the Bessel function of the first kind.

The corresponding energies of the Wannier-Stark states are

$$\epsilon_{\alpha l} = \varepsilon_\alpha + leaF_x \ . \tag{15}$$

These energies are equidistant and form the so-called Wannier-Stark ladder[36–38] with the levels separated by the Bloch-oscillation frequency

$$\omega_B = eaF_x/\hbar \ . \tag{16}$$

This spacing physically corresponds to the energy needed to move an electron by one lattice constant in the field direction. Thus, in the constant (or, adiabatic) electric field, the electron spectrum of the system is universal: each band gives rise to a Wannier-Stark ladder with the same level spacing $\hbar\omega_B$. While the form of the Wannier-Stark wave functions Eqs. (13) or (14) are specific for the tight-binding approximation, i.e., model-dependent, the energy spectrum of the Wannier-Stark states depends only on the lattice constant and is model-independent.

In a time-dependent electric field $F_x(z,t)$, it is convenient to solve the Shrödinger equation (11) using an adiabatic basis of the time-dependent eigenfunctions $\tilde{\phi}_{\alpha l}(k,z,t)$ and the corresponding eigenenergies $\epsilon_{\alpha l}(z,t)$, which acquire their time dependence due to that of $F_x(z,t)$. These adiabatic basis wave functions we chosen as

$$\tilde{\Phi}_{\alpha l}(k,z,t) = \exp\left[-\frac{i}{\hbar}\int \epsilon_{\alpha l}(z,t)dt\right]\tilde{\phi}_{\alpha l}(k,t,z) \ , \tag{17}$$

where we have explicitly indicated the evolutionary exponent due to the phase accumulation of the adiabatic solution.

We emphasize that this adiabatic basis describes a system of uncoupled Wannier-Stark ladders of different bands and does not take into account the coupling between them due to the Zener tunneling[39]. We will call it an uncoupled adiabatic basis. It is different from the complete adiabatic basis, which is a solution of the full Scrödinger equation in a stationary (adiabatic) external field.

We perform a discreet Fourier transform of the adiabatic basis wave functions (17) from the integer variable l to "quasi-momentum" $-\pi < q \leq \pi$ defined as

$$\tilde{\Phi}_{\alpha q}(k,z,t) = \sum_l \frac{e^{-iql}}{\sqrt{L}}\tilde{\Phi}_{\alpha l}(k,z,t) \ . \tag{18}$$

Then the solution of the Schrödinger equation (11) can be expressed in the following form

$$\phi_\alpha(k,z,t) = \sum_q \beta_\alpha(q,z,t)\Phi_{\alpha q}(k,z,t) \ , \tag{19}$$

where β_α are expansion coefficients, which satisfy the following system of equations

$$\frac{d\beta_\alpha(q,z,t)}{dt} = i\mu_\alpha(t,z)\beta_\alpha(q,z,t) - i\frac{F_x(z,t)}{\hbar}\sum_{\alpha'} Z_{\alpha\alpha'}\kappa_{\alpha\alpha'}\beta_{\alpha'}(q,z,t) \ . \tag{20}$$

Here

$$\mu_\alpha(z,t) = -\frac{d\gamma_\alpha}{dt}\sin\left(q + \frac{ea}{\hbar}\int F_x(z,t)dt\right) \tag{21}$$

and

$$\kappa_{\alpha\alpha'} = \exp\left\{i\left[t\frac{\epsilon_\alpha - \epsilon_{\alpha'}}{\hbar} + (\gamma_{\alpha'} - \gamma_\alpha)\sin\left(q + \frac{ea}{\hbar}\int F_x(z,t)dt\right)\right]\right\} \ , \tag{22}$$

where, as everywhere else in this article, $\alpha, \alpha' = 1, \ldots, N_{\text{bands}}$.

Eliminating the diagonal terms from the system (20) via the following substitution

$$\beta_\alpha(q,z,t) = \hat{\beta}_\alpha(q,z,t)e^{i\int \mu_\alpha dt}, \tag{23}$$

we obtain the final system of equations, which describes coupling of the states of the conduction and the valence bands,

$$\frac{d\hat{\beta}_\alpha(q,z,t)}{dt} = -i\frac{F_x(z,t)}{\hbar}\sum_{\alpha'\neq\alpha} Q_{\alpha\alpha'}(q,z,t)\hat{\beta}_{\alpha'}(q,z,t) \ , \tag{24}$$

where we have denoted

$$Q_{\alpha\alpha'}(q,z,t) = Z_{\alpha\alpha'}\exp\left\{i\left[t\frac{\epsilon_\alpha - \epsilon_{\alpha'}}{\hbar} + \frac{\Delta_\alpha - \Delta_{\alpha'}}{2\hbar}\int_{-\infty}^{t} dt_1 \cos\left(q + \frac{ea}{\hbar}\int_{-\infty}^{t_1} F_x(z,t_2)dt_2\right)\right]\right\} \ . \tag{25}$$

The system of equations (24)-(25) describe dynamics of an electron in an external time-dependent electric field within the N_{bands}-band approximation.

Combining all terms in the definition of function $\Phi_{\alpha q}(k,z,t)$, one can derive that the solution of the Shrödinger equation [see Eq. (19)], can be also expressed in term of the Houston functions[40] $\Phi^{(H)}_{\alpha q}(k,z,t)$,

$$\phi_\alpha(k,z,t) = \sum_q \hat{\beta}_\alpha(q,z,t)\Phi^{(H)}_{\alpha q}(k,z,t) \ , \tag{26}$$

where

$$\Phi^{(H)}_{\alpha q}(k,z,t) = \tilde{\delta}\left(k - k_F(t)\right) \times \\ \times \exp\left\{-i\left(t\frac{\epsilon_\alpha}{\hbar} + \frac{\Delta_\alpha}{2\hbar}\int^t dt_1 \cos\left[k_F(t_1)a\right]\right)\right\}, \quad (27)$$

where the time-dependent wave vector is defined as

$$k_F(t) = \frac{q}{a} + \frac{e}{\hbar}\int^t F_x(z,t_1)dt_1, \quad (28)$$

$\tilde{\delta}(k) = \sum_n \delta(k + 2\pi n/a)$ with summation over integer n, and $\delta(k)$ is the Dirac delta-function.

The system of equations (24)-(25) is applicable to an electronic system with any number of bands $N_{\rm bands}$. For simplicity, below we consider only two bands: one valence band and one conduction band, i.e., $N_{\rm bands} = 2$. Such two-band system captures main features of the propagation of an ultrashort optical pulse through a dielectric film. We assume that the dielectric is silica with the parameters of the Hamiltonian corresponding to the band structure of silica[41]. Namely, we choose $\varepsilon_c = 0$, $\varepsilon_v = -11.25$ eV, $\Delta_v = 0.5$ eV, and $\Delta_c = -4.0$ eV. Such values of the parameters determine the band gap of silica equal to 9 eV.

An additional parameter, which characterizes the electron dynamics, is the interband dipole matrix element Z_{vc}. For a two-band system, there is only one such a parameter corresponding to the dipole coupling of the CB and VB. It is obvious that $Z_{vc} \lesssim ea \sim 5$ eÅ, where we assume that the lattice constant of silica is $a = 5$ Å. Correspondingly, we will mostly use below values for this parameter $Z_{vc} = 1$ eÅ and $Z_{vc} = 3$ eÅ. Note that eÅ ≈ 4.8 debye.

A unique feature of the coherent dynamic equations (24) is that the interband coupling is realized only between the states with the same value of quasimomentum q. This property strongly simplifies the problem, since now we only need to solve the finite system of two-component (in this case of a two-band electron system) first-order differential equations.

The relaxation processes, which take place on a longer time scale, $t \gtrsim \tau_e \sim 20$ fs, would lead to population transfer between states with different q. In such a case purely Schrödinger description of the dynamics would be impossible and the dynamics could be described using, e.g., density matrix equations.

With the known time-dependent electric field $F_x(z,t)$, the system of equations (24), for each value of q, determines the temporal evolution of the dressed electronic states (in the Houston-function representation)

$$\mathcal{B} = (\hat{\beta}_v, \hat{\beta}_c)\ , \quad (29)$$

where $\hat{\beta}_v$ and $\hat{\beta}_c$ are amplitudes to be in the VB and the CB, respectively.

For such states, there are two types of initial conditions, $\mathcal{B}^{(v)} = (1,0)$ and $\mathcal{B}^{(c)} = (0,1)$, which correspond to the evolution of the dressed states of the VB and CB, respectively. During this temporal evolution, all the dressed states $\mathcal{B}^{(v)}(t)$ are occupied by electrons, while all the dressed states $\mathcal{B}^{(c)}(t)$ remain empty. Although the dressed states $\mathcal{B}^{(v)}(t)$ initially correspond to the pure VB states, at later times they are a mixture of the initial (unperturbed) VB and CB states.

Such a mixing of the valence and conduction bands results in polarization (i.e., an oscillating optical dipole-moment density) of the system. This polarization's vector has only x components and is determined by the dressed states $\mathcal{B}^{(v)}$ only and has the following form

$$P_x(z,t) = \frac{1}{2\pi a^3} \times \\ \int_{-\pi}^{\pi} dq \left[\mathcal{B}^{(v)\dagger}(q,z,t)\hat{Q}(q,z,t)\mathcal{B}^{(v)}(q,z,t) + \text{c.c.}\right]\ , \quad (30)$$

where $\hat{Q}$ is a matrix with elements $Q_{\alpha\alpha'}$ – see Eq. (25). Such a polarization should be substituted into the Maxwell equation (5), which finally closes the system of equations (2)-(5), (24), (30), self-consistently describing the propagation of ultrashort pulse through the dielectric system.

Similar system of equations were introduced to describe the propagation of electromagnetic pulses through two-level systems – see, e.g. Refs. 42,43. For a two-level system, the corresponding system of equations is a combination of the Maxwell equations and the Bloch equations. Our system of equations, which describe the electron dynamics in the two-band approximation, becomes similar to the Bloch equations for two-level systems if the bandwidths, Δ_α, are set to zero. In contrast to the two-level (resonant atomic) systems, the quantum evolution of a solid is significantly dependent on the finite bandwidths – see Eq. (25) – that determine the adiabatic phase, $\frac{ea}{\hbar}\int F_x(z,t)dt$, associated with transitions between the Wannier-Stark levels.

III. ADIABATIC STATES IN EXTERNAL ELECTRIC FIELD

A. Adiabatic states of coupled two-band system

The physical picture of the unfolding processes can be understood in terms of the full adiabatic states of the coupled-band system, which are different from those for the *uncoupled* bands introduced in Sec. II B. Such full adiabatic states are defined as solutions of Eq. (11) at a constant electric field F_x. It is convenient to use the Wannier-Stark functions $\phi_{\alpha l}(k)$ as the basis functions and express an adiabatic state Ψ in the following form

$$\Psi = \sum_{\alpha l} \Lambda_{\alpha l}\phi_{\alpha l}(k). \quad (31)$$

Then from Eq. (11) we obtain that the coefficients $\Lambda_{\alpha l}$ satisfy the following equation:

$$E\Lambda_{\alpha l} = (\varepsilon_\alpha + leaF_x)\,\Lambda_{\alpha l} + F_x \sum_{\alpha' l'} Z_{\alpha\alpha'} J_{|l-l'|}(\gamma_\alpha - \gamma_{\alpha'})\Lambda_{\alpha' l'} \ , \quad (32)$$

where E is the eigenenergy corresponding to Ψ. This expression of the interband coupling in terms of the Bessel functions is a characteristic feature of the tight-binding approximation.

The Wannier-Stark states are characterized by an integer index l, which can be considered as the number of the lattice site at which a given Wannier-Stark state is localized. The second term in right-hand side of Eq. (32) describes the coupling between the localized Wannier-Stark states of different bands, which is defined by the function

$$J_{|l-l'|}(\gamma_\alpha - \gamma_{\alpha'}) = J_{|l-l'|}\left(\frac{\Delta_\alpha - \Delta_{\alpha'}}{2eaF_x}\right), \quad (33)$$

which depends on the "distance" $|l-l'|$ between the localized Wannier-Stark states and on the difference of the bandwidths $\Delta_\alpha - \Delta_{\alpha'}$.

In contrast to the electron wave functions without external electric field, which are delocalized Bloch states, the Wannier-Stark states are localized along the direction of external electric field. The localization length of the Wannier-Stark states, as follows from Eq. (14), is

$$L_{WS} \sim \frac{\Delta_\alpha}{|eF_x|} \ . \quad (34)$$

Due to the localized nature of the Wannier-Stark states, we can conclude that the interband coupling is the strongest for the nearest-neighbor Wannier-Stark states. Indeed, at a strong electric field, $ea\,|F_x| \gtrsim \Delta_\alpha$ (or, $L_{WS} \lesssim a$), the interband coupling has the largest value at $\Delta l = l - l' = \pm 1$ and monotonically decreases with increasing Δl. For instance, assuming a realistic value $\Delta_\alpha = 4.5$ eV, the strong electric field is $\gtrsim 0.2$ V/Å.

Strong mixing of the Wannier-Stark states of different bands takes place when the energy separation between the corresponding Wannier-Stark states is comparable to the interband coupling, i.e., under the condition of anticrossing of the Wannier-Stark levels. From Eq. (15) it follows that the anticrossing condition of two Wannier-Stark states belonging to conduction and valence bands acquires the form

$$\varepsilon_c - \varepsilon_v = a\,|eF_x \Delta l| \, . \quad (35)$$

Hence, for all members of the Wannier-Stark ladder, anticrossings occur simultaneously.

The magnitude of the anticrossing gap is determined by the value of the interband coupling (33) at $\Delta l = (\varepsilon_c - \varepsilon_v)/|eaF_x|$. Such coupling is strongest for the minimum value of $\Delta l = 1$, i.e., for the largest F_x.

With an increasing external field F_x, the two-band system undergoes successive anticrossings corresponding to decreasing values of Δl [see Eq. (35)]: $F_x \approx (\varepsilon_c - \varepsilon_v)/|e|a\Delta l$. Note that the approximate nature of this relation is due to the fact that a strong coupling causes shifting of the anticrossing points with respect to the values of Eq. (35) expected for the weak coupling. The final and strongest (with the maximum gap) anticrossing occurs at $\Delta l = 1$ at an electric field $F_x \approx (\varepsilon_c - \varepsilon_v)/|e|a$.

To illustrate relative strengths of the anticrossing gaps, we show in Fig. (2) the energy levels of a finite two-band system consisting of 50 crystallographic planes in the field direction; correspondingly, there are 50 Wannier-Stark states in each of the two (valence and conduction) Wannier-Stark ladders. This energy spectrum is calculated from Eq. (32). Two sets of anticrossings are clearly visible. These correspond to $\Delta l = 1$ (at $F_x \approx 2.6$ V/Å) and $\Delta l = 2$ (at $F_x \approx 1.1$ V/Å), i.e., the anticrossings of the nearest neighbor and the next-nearest neighbor Wannier-Stark levels of the conduction and valence bands. The largest gap at the $\Delta l = 1$ anticrossing illustrates the strongest interband coupling for the nearest-neighbor Wannier-Stark states.

Within an optical half-cycle of the time-dependent field of a strong optical pulse, the Wannier-Stark levels can experience a number of anticrossings as the field increases (corresponding to $|\Delta l| = N_p - 1, N_p - 2, \ldots, , 2, 1$, where N_p is the number of the crystallographic planes in the direction of the field), and then the same number of the anticrossings occur as the field decreases. The passage of any such an anticrossing corresponding to a given Δl will be adiabatic if $\hbar\omega_0 \ll \Delta E_{ac}$ (where ΔE_{ac} is the corresponding anticrossing splitting) and diabatic in the opposite limiting case – see Sec. IV B.

B. Wannier-Stark levels in adiabatic field

The analysis of the previous section is based on the picture of the Wannier-Stark states and anticrossing of such states when the electric field is varied. Such analysis is valid only if it is enough time for the time-dependent electric field to form the Wannier-Stark states. To analyse the formation of the Wannier-Stark states we consider in this section a single-band system, which is characterized by zero offset energy, $\varepsilon_1 = 0$, and finite band width, Δ_1.

The condition of formation of Wannier-Stark states can be expressed in a following way. The physical origin of Wannier-Stark localization and quantization is the interference of electron packages, first accelerated by electric field and then reflected from the periodic lattice potential. The motion of an electron with 1D wavevector k, pointing along the direction of electric field, is described by the following equation

$$\frac{dk}{dt} = \frac{e}{\hbar}F. \quad (36)$$

The electron motion in reciprocal space is restricted by

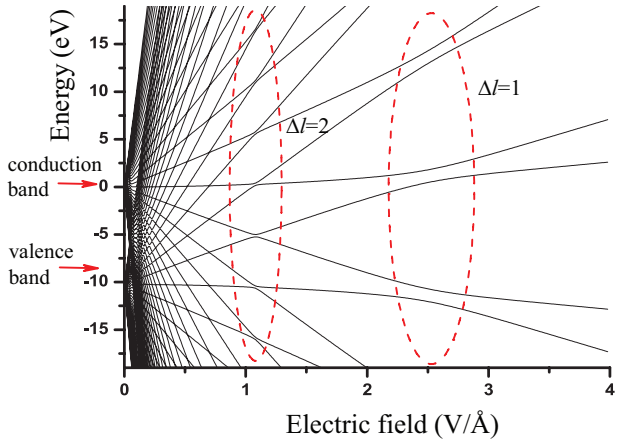

FIG. 2: Energy spectra of two-band system as a function of external uniform electric field. The two bands correspond to valence and conduction bands of silica with the energy gap of 9 eV. The band edges are shown by arrows, and anticrossings are marked by red ovals. Only the strongest anticrossings, corresponding to $\Delta l = \pm 1$ and $\Delta l = \pm 2$, are shown. The anticrossing gap is the strongest for $\Delta l = \pm 1$.

the values of k within the first Briullien zone, i.e., $-\pi/a < k < \pi/a$. Therefore, the wavevector k, after reaching the point π/a following equation of motion (36), will be Bragg-reflected to the point $-\pi/a$. Such reflections result in periodic Bloch motion of electron in reciprocal space with the period

$$T_B = \frac{2\pi}{\omega_B} \ . \tag{37}$$

Therefore, the time of formation of Wannier-Stark states is the period of Bloch oscillations, T_B. This time should be compared to the rate of change of electric field to determine the applicability of description in terms of Wannier-Stark states. For example, for $F = 2$ V/Å and $a = 5$ Å the period of Bloch oscillations is $T_B \sim 0.4$ fs.

The wave functions, introduced in Sec. IIB to describe the electron dynamics, are the Houston functions (27), which at zero electric field are Bloch functions and at finite electric field depend on time t through the time-dependent wavevector, $k_F(t)$. Even at constant electric field, these functions are not stationary: they depend on t and contain information about the stationary Wannier-Stark functions. To demonstrate this, we perform a sliding Fourier transform of the Houston function (27)

$$\psi_{lq}(x,t) = \int_{t-\Delta t/2}^{t+\Delta t/2} dt' e^{il\omega_B t'} \int_{-\infty}^{\infty} \frac{dk}{2\pi} e^{-ikx} \Phi_q^{(H)}(k,t') \ . \tag{38}$$

In Fig. 3, we show the driving field $F(t)$ as a function of time t [panel (a)] and the time-dependent wave functions $\psi_{lq}(x,t)$ for $q = 0$ (i.e., originating from the Γ-point of the Brillouin zone) for two moments of time t: when field F near its maximum, $F = 2.1$ V/Å [panel (b)] and

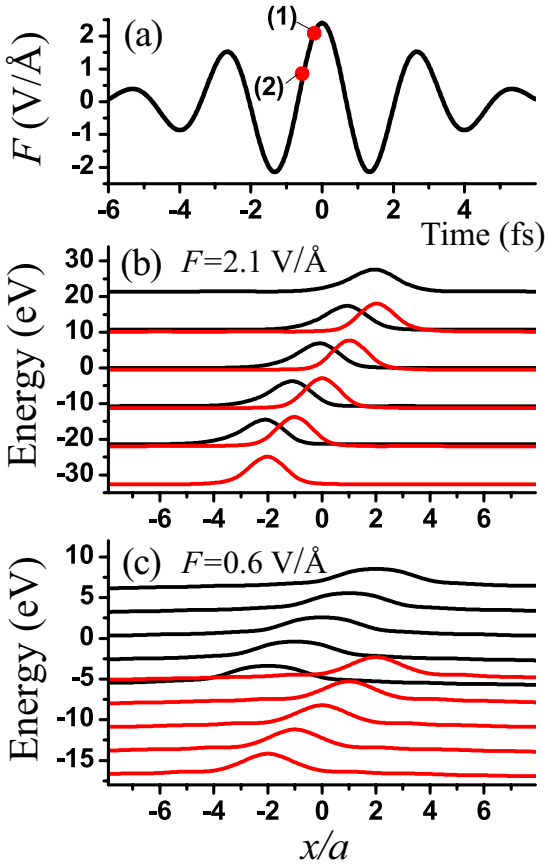

FIG. 3: Driving electric field and localized electronic states. (a) Electric field of an optical pulse with frequency $\hbar\omega_0 = 1.5$ eV and pulse length $\tau_p = 4$ fs as a function of time t. The electronic states were computed at points in time 1 and 2 with instantaneous fields $F = 2.1$ VÅ and $F = 0.6$ VÅ, respectively, marked by the red dots. (b) Sliding Fourier transform (38) of the Houston functions (27) calculated for instantaneous field $F = 2.1$ VÅ at the energies of the Wannier-Stark ladder $E_l = l\hbar\omega_B$, where l is integer. The curves are displaced vertically according to E_l. The red and black colors denote the VB and CB ladders, correspondingly. The width of the time window of the sliding Fourier transform is $\Delta t = 0.5$ fs. (c) The same as (b) but for $F = 0.6$ VÅ.

at the moment when F is relatively low, $F = 0.6$ V/Å [panel (c)]. In all cases, these wave functions are well-defined Wannier-Stark localized states. For a strong field [Fig. 3(b)] their localization is much stronger than for a moderate field [Fig. 3(b)], as expected. Also, the spatial width of these wave functions in the CB is significantly greater than in the VB because the CB energy width is much greater, in accord with Eq. (14).

In such a way, we can assume that for $F \gtrsim 1$ V/Å the description of electron dynamics in terms of Wannier-Stark states is applied. This is the range of electric field, within which the strong anticrosssings of Wannier-Stark levels of different bands are expected.

IV. RESULTS AND DISCUSSION

A. Enhancement of reflection of the optical pulse

A strong optical pulse propagating through a dielectric film causes nonlinear modification of its electronic system, which through the dielectric polarization P_x changes the propagation of optical pulse itself selfconsistently. Consequently, the reflectance of the strong pulse should significantly depend on the intensity of the pulse, i.e., on its peak electric field, F_0.

Consider a moment of time t_f when the reflected and transmitted pulses are well separated as ishown in Fig. 4 for a 100 nm dielectric film. Both the pulses, reflected and transmitted, have the shapes similar to that of the incident pulse and propagate away from the film. Reflectance $\mathcal{R}$, which is defined as the reflected fraction of the optical pulse energy, is calculated from the following expression

$$\mathcal{R} = \frac{\int_{-\infty}^{0} dz |F_x(z, t = t_f)|^2}{\int_{-\infty}^{0} dz |F_x(z, t = 0)|^2}, \tag{39}$$

where $z = 0$ is the coordinate of the left boundary of the dielectric film. It is assumed that the incident pulse is generated at $t = 0$ far away from the film.

In a similar way, we can calculate absorption of the optical pulse as the fraction of its absorbed energy. For the pulse intensity $\mathcal{P}$ not too high, i.e., for the intensity smaller than the breakdown threshold intensity, $\mathcal{P}_B \approx 2.5 \times 10^{14}$ W/cm^2 for a few-femtosecond pulse, our calculations indicate (results not shown) that the absorbance $\mathcal{A}$ of the pulse in a thin dielectric nanofilm is small, $\mathcal{A} \lesssim 1 - 2$ %. This is much smaller than the reflectance of the pulse, $\mathcal{R} \sim 20$ %. This fact suggests that the interaction of the ultrashort strong pulse with the dielectric is reversible, non-damaging.

The reflectance $\mathcal{R}$ depends also on the thickness h of the film, which is due to interference of the transmitted optical wave with that reflected from the back boundary of the film. In Fig. 5(a), the dependence of the reflectance on the thickness of the film is shown for two pulses with different intensities. The reflectance is small for a small thickness of the film, and it reaches its maximum value at a finite thickness h, which is a behavior characteristic of a very thin Fabry-Pérot interferometer (this is a part of the first Fabry-Pérot oscillation). This maximum is reached at $h \sim \lambda/n_{\text{eff}}$, where n_{eff} is the effective refractive index of the film. In this maximum, an analytical solution of the Maxwell equations yields the following expression for the reflectance[44],

$$\mathcal{R}_{\max} \approx \left(\frac{1 - n_{\text{eff}}^2}{1 + n_{\text{eff}}^2} \right)^2 . \tag{40}$$

The reflectance shown in Fig. 5(a) increases from $\mathcal{R} = 13\%$ to $\mathcal{R} = 25\%$ when the field amplitude increases from $F_0 = 0.1$ V/Å to $F_0 = 3.5$ V/Å. This corresponds to the

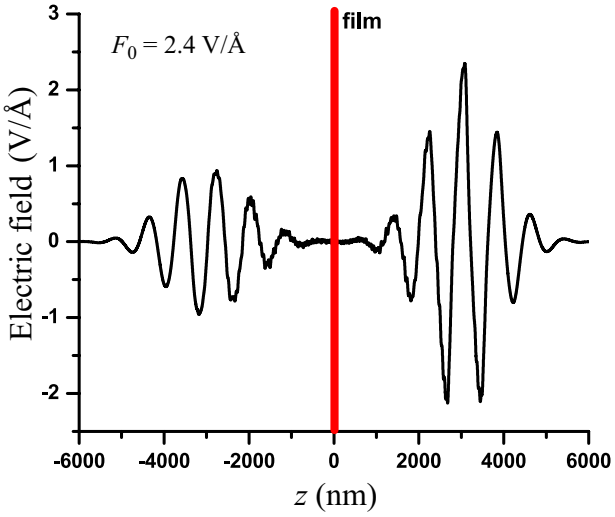

FIG. 4: Spatial distribution of the electric field of the pulse at a moment of time when the laser pulse just passed through the dielectric film. The well-formed transmitted and reflected pulses are clearly visible. The pulses propagate away from dielectric film, which is shown schematically by red line. The peak electric field of the incident pulse is 2.4 V/Å. The thickness of the dielectric film is 100 nm. The reflectance of the pulse is $\mathcal{R} = 19$ %.

increase of the effective index (40) from $n_{\text{eff}} = 1.46$ to $n_{\text{eff}} = 1.73$, i.e., the effective index change is $\Delta n_{\text{eff}} = 0.2$. To compare, with the known Kerr constant for silica[45] $n_2 = 3.2 \times 10^{-16}$ cm^2/W and the peak pulse power $P_0 = 1.6 \times 10^{14}$ W/cm^2 (corresponding to $F_0 = 3.5$ V/Å), the Kerr-effect increase of the index would have been $\Delta n_{\text{eff}} = 0.05$, i.e., significantly less than predicted by the present theory – see Fig. 5 (b) where the black curve displays the theory prediction, and the red one shows the Kerr-effect reflectance. This implies that in high fields the dielectric (silica) becomes much more polarizable ("softer") than expected from the low-field behavior. This softening is interpreted as a precursor to the adiabatic metallization[11,13], which is incomplete because the present field is too fast to be adiabatic.

In Fig. 6 we display polarization relative to the maximum pulse field $\chi_{\text{eff}} = P_x/F_0$; note that $\varepsilon_{\text{eff}} = \max[4\pi |\chi_{\text{eff}}|]$ is the corresponding contribution to effective maximum permittivity. This relative polarization is computed for the mid-plane of a $h = 100$ nm nanofilm and for the optical pulse with peak value of $F_0 = 2.4$ V/Å. This effective permittivity contribution is significant, $\varepsilon_{\text{eff}} \approx 2.5$, which again implies the field-induced softening of the dielectric.

The increase of the refractive index in a strong external electric field of the optical pulse is due to generation of non-linear internal polarization, P_x, of the system. Such polarization is determined by the nonlinear mixture of the states of the valence and conduction bands. Such a mixture can be described in the basis of the Wannier-

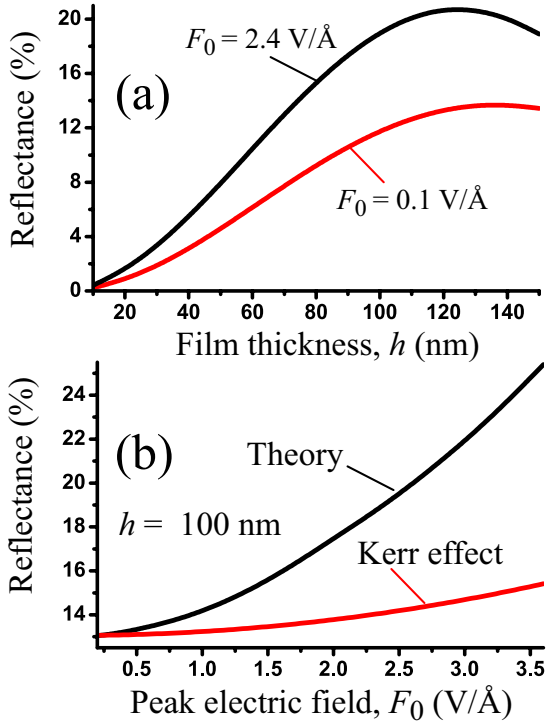

FIG. 5: (a) The reflectance of the laser pulse as a function of the thickness of the silica film is shown for two pulses with high (black line) and low (red line) intensities with corresponding peak electric field values $F_0 = 2.4$ V/Å and $F_0 = 0.1$ V/Å (red line). (b) The reflectance of the laser pulse as a function of the peak electric field of the pulse is shown for the 100 nm dielectric film (black line). A reflectance prediction from the Kerr effect (red line) – see the text: Eq. (40) and below.

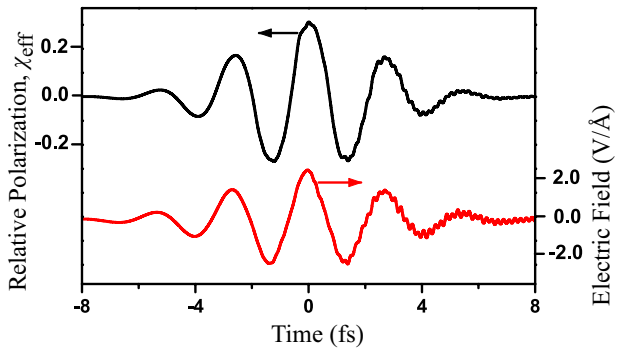

FIG. 6: Time-dependent relative polarization $\chi_{\rm eff} = P_x/F_0$ for silica film of $h = 100$ nm thickness calculated from Eq. (30) for laser pulse with the amplitude of 2.4 V/Å (black curve). Electric field of the pulse as a function of time (red curve). Both the polarization and the field are calculated in the mid-plane of the dielectric film.

Stark states. In this basis, the interband coupling is a nonlinear function of electric field and is the strongest near the anticrossing points of the Wannier-Stark energy ladders.

To illustrate this effect, consider the adiabatic levels of the system (see Sec. III) shown in Fig. 7 where we display a small fragment of the band diagram of Fig. 2 in an intermediate region of fields along with interband dipole transitions denoted by the vertical arrows and population of the filled and empty states indicated by filled and empty circles, respectively.

Figure 7 (a) illustrates a case of the diabatic passage of the level anticrossings, where this passage occurs so rapidly that these anticrossings are ignored by the system. The condition of the diabatic passage is $\delta \gg 1$ where $\delta = \hbar\omega/\Delta_{ac}$ is the so-called adiabatic parameter, and Δ_{ac} is the anticrossing splitting energy. In Fig. 7 (a), the crossed arrows indicate the direction in which the populations and wave functions are preserved through the anticrossings. As one can see from the energy scale, in the vicinity of the anticrossings, there are allowed transitions (i.e., those between the empty and filled levels) in the near-infrared/visible (nir-vis) spectral region, i.e., within the spectral width of the excitation pulse. These transitions are responsible for the polarization discussed above in conjunction with Fig. 6. As one can see, all the transitions in this case occur between the terms that are not parallel, which in accord with Eq. (35) implies that the corresponding Wannier-Stark states are localized at different lattice sites. Given that at such fields these states are strongly localized (cf. Fig. 3), the overlap of the wave functions of such states localized at different sites is relatively small. Therefore the dipole transitions between them are suppressed and the corresponding polarization is not large. This appears to be the case for the conditions under consideration.

The opposite limiting case of the adiabatic (i.e., for $\delta \ll 1$) passage of the anticrossings is illustrated in Fig. 7 (b). In this case, the population stays on a continuous line (term), as the curved arrows indicate, while the wave functions are exchanged when an anticrossing is passed. Such an exchange implies transfer of the electron population in space between different lattice sites. As a result, there are strong transitions between parallel terms, i.e., between the Wannier-Stark states localized at the same lattice site. One such a transition is indicated by the bold red arrow in Fig. 7 (b). These transitions, which appear due to adiabatic population transfer, are analogous to those appearing due to metallization of dielectric nanofilms[11,13].

In Fig. 8, we show the temporal dynamics of the incident pulse field (black curve) and that of the field inside the dielectric (at the mid plane of the nanofilm) shown by the red curve. This internal field is of importance since it self-consistently determines electron dynamics in the dielectric. This field is suppressed compared to the field of the incident pulse due to reflection from the dielectric-vacuum interface. This reflection is enhanced because of

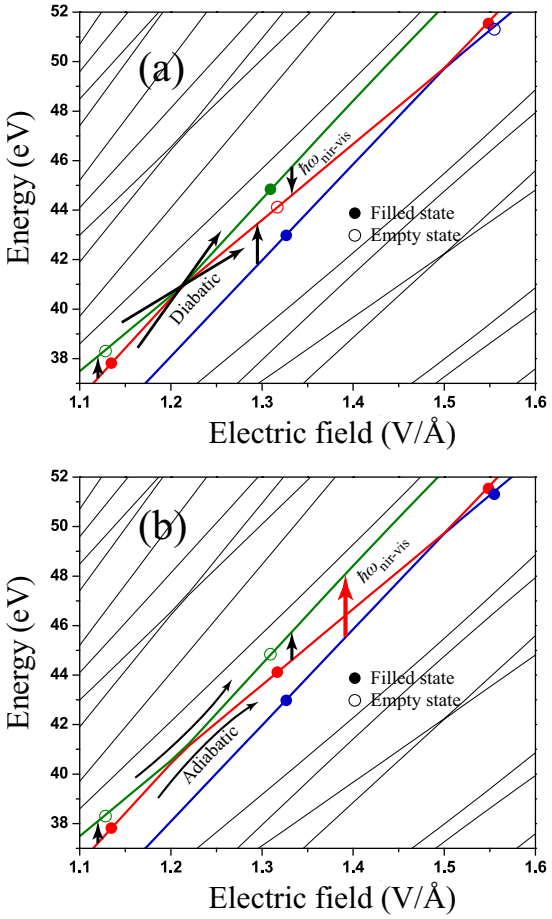

FIG. 7: Fragment of the adiabatic energy levels of the nanofilm as function of the applied electric field. The vertical arrows indicate allowed dipole transitions in a near-infrared/visible frequency region. The arrows at the anticrossing points show pathways of the passage of the anticrossings. The open (filled) circles denote empty (filled) states. The line color codes the order of levels in their energy. (a) Diabatic passage: at the anticrossing point the states with the given quantum numbers preserve their population. The crossed arrows indicated the directions in which the population is preserved. (b) Adiabatic passage: the population is conserved for both the lower and upper levels as indicated by the curved arrows. The bold red arrow shows the strongest transition that occurs between the parallel levels (terms) corresponding to the Wannier-Stark states localized at the same lattice site, one of which is empty and the other populated.

the polarizability of the dielectric is increased due to the enhanced nonlinear effects both in the diabatic and adiabatic pathways – see above the discussion of Fig. 7. Note that the internal field pulse (the red line) is almost (but not perfectly) symmetric with respect to its maximum point, which implies that the excitation of the dielectric by the strong field is almost reversible: very little population of the CB is left behind after the pulse ends. Nevertheless, there is some small but appreciable asymmetry of the internal field pulse with respect to its maximum:

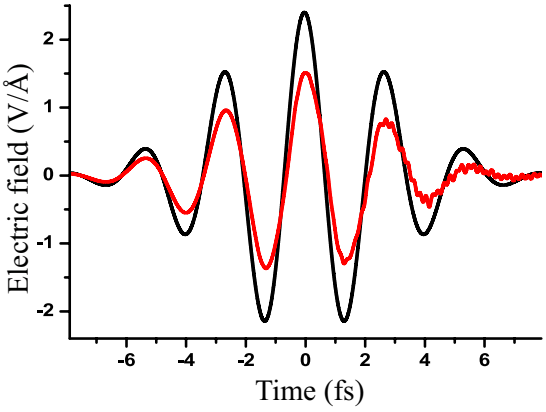

FIG. 8: The electric field of the incident optical pulse (black line) and the electric field at the midpoint of the dielectric film (red line) are shown as functions of time. The graphs are shifted in time so that the maxima of two dependencies occur at the same moment of time. The thickness of the film is 100 nm and the amplitude of the laser pulse is $F_0 = 2.4$ V/Å.

on the trailing edge the internal field is somewhat smaller compared to that at the leading edge implying that a relatively small population is left behind by the strong pulse – see also below Fig. 9 and its discussion.

B. Dynamics of electron system

The electric field of the optical pulse induces mixing of the electronic states of the VB and CB. The amplitudes for an electron to be in the VB or CB is given by projection of its exact time-dependent wave function onto the unperturbed states of the corresponding band (VB or CB). The occupied electron states, which are initially the valence band states, are represented by wave functions $\mathcal{B}^{(v)} = \left(\hat{\beta}_v^{(v)}, \hat{\beta}_c^{(v)}\right)$ [see Eq. (29) above] and have both the VB and CB components. The CB occupation $\mathcal{N}_c(t)$ is given by

$$\mathcal{N}_c(t) = \int dz \int dq \left|\hat{\beta}_c^{(v)}(q, z, t)\right|^2 , \qquad (41)$$

where the integral over momentum q is extended over the first Brillouin zone, and the z-integral is extended over the nanofilm thickness. The conduction band population of Eq. (41) is a fundamentally observable quantity, though in practice it may not be easily measurable. Physically, $\mathcal{N}_c$ determines such a particularly important effect as Pauli blocking of the VB to CB transitions.

The occupation $\mathcal{N}_c$ of the CB states is shown in Fig. 9 for the interband dipole parameter $Z_{vc} = 3.0$ eÅ and amplitude of the optical pulse $F_0 = 2.4$ V/Å. The conduction band occupation $\mathcal{N}_c$ is clearly behaving as a function of the instantaneous electric field of the pulse, more precisely of $|F(t)|$. This occupation has its maximum values at the maxima and minima of the pulse electric

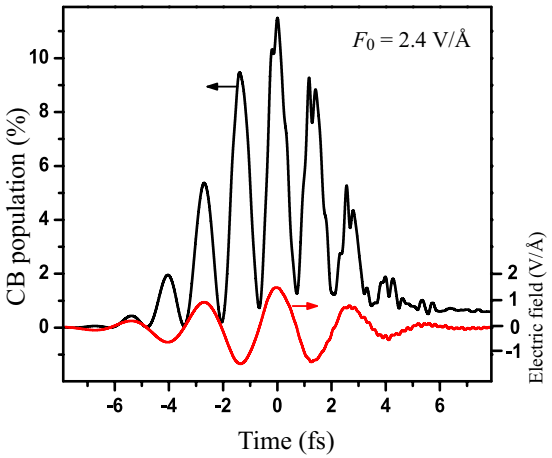

FIG. 9: The time-dependent conduction band population, defined by Eq. (41), is shown for dielectric film with the thickness of 100 nm. The amplitude of the pulse is 2.4 V/Å. The electric field at the midpoint of the film is also shown. There is a correlation between the the conduction band population and electric field of the pulse. There is also small residual population, illustrating that the electron system almost returns to the original state after the pulse passes through the film. The interband dipole matrix element is $Z_{vc} = 3.0$ eÅ.

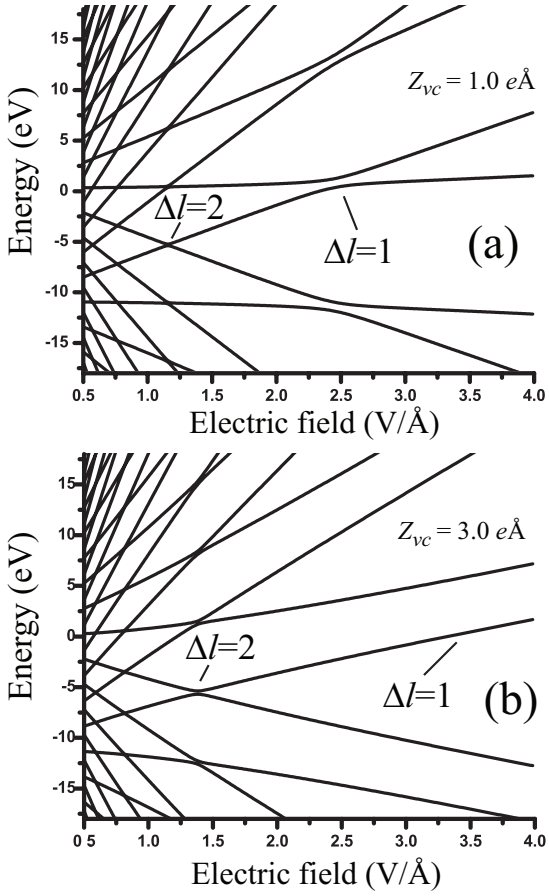

FIG. 10: Adiabatic energy spectra of two-band system is shown as a function of external electric field for different values of Z_{vc}: (a) $Z_{vc} = 1.0$ eÅ, and (b) $Z_{vc} = 3.0$ eÅ. The two bands are the VB and CB of silica with the energy gap $\Delta_g = 9$ eV. This two-band system is finite and each band consists of 50 energy levels. The anticrossing points with $\Delta l = 1$ and $\Delta l = 2$ are shown.

field. In addition to a smooth time-dependent part of $\mathcal{N}_c$, which follows $|F(t)|$, there are also fast oscillations with frequency close to the $\Delta_g/\hbar$, where Δ_g is the bandgap. There is also a small, $\approx 0.5\%$, residual population of the CB after the pulse passes through the film. This smallness of the residual population is due to the circumstance that both the pure diabatic and adiabatic passages of the anticrossings do not leave the residual population. In our case, this residual population, as well as the fast population oscillations, are likely to be due to impure diabatic passages (i.e., the passages that are fast but not infinitely fast). Note that oscillations of a similar nature are also seen in the polarization and internal field – see Fig. 6.

Above in this Section, we have considered the electron dynamics for a fixed interband matrix element $Z_{vc} = 3$ eÅ. There is a nontrivial dependence of the electron dynamics on this matrix element that we will discuss below.

In Fig. 10 (a), results are shown for a relatively low dipole interband coupling, $Z_{vc} = 1.0$ eÅ. For an anticrossing at $\Delta l = 2$ (the next-nearest neighbor), the anticrossing splitting (gap) is very small $\Delta_{ac} \approx 0.03$ eV; correspondingly $\delta \gg 1$, and the passage is extremely diabatic. For the anticrossing at $\Delta l = 1$ (the nearest neighbor anticrossing, which occurs last as the electric field increases), $\Delta_{ac} \approx 1$ eV. With $\hbar\omega_0 = 1.5$ eV, $\delta \sim 1$, and the passage of this last anticrossing is intermediate between diabatic and adiabatic; consequently, one can expect a significant residual CB population to occur (see also discussion below in Sec. V).

The corresponding dynamics of the CB population for this low interband coupling matrix element $Z_{vc} = 1.0$ eÅ is displayed in Fig. 11 (a). As we see, both the maximum population (at $t \approx 2$ fs) and the residual CB population (for $t > 6$ fs) monotonously increase with the excitation field amplitude F_0. The CB population (both maximum and residual) becomes very large, $\mathcal{N}_c \approx 20 - 40\%$, for $F_0 \geq 2.8$ V/Å leading to an increased deposition of energy and possible dielectric breakdown.

The adiabatic levels for a larger dipolar coupling, $Z_{vc} = 3.0$ eÅ, are illustrated in Fig. 10 (b). Note that anticrossings for a given Δl are shifted to higher fields with respect to the case of low dipolar coupling [cf. Fig. 10 (a)]. For the anticrossing at $\Delta l = 2$, $\Delta_{ac} \approx 0.3$ eV and $\delta \approx 5$; thus the passage of this anticrossing is mostly diabatic. In contrast, for $\Delta l = 1$, $\Delta_{ac} \approx 5$ eV and $\delta \approx 0.3$; hence, this anticrossing is mostly adiabatic. However, it occurs at a very high field $F_0 = 3.5$ V/Å where electric breakdown is likely to occur even for such short excitation pulses [see also below in the discussion of Fig. 12 (b)

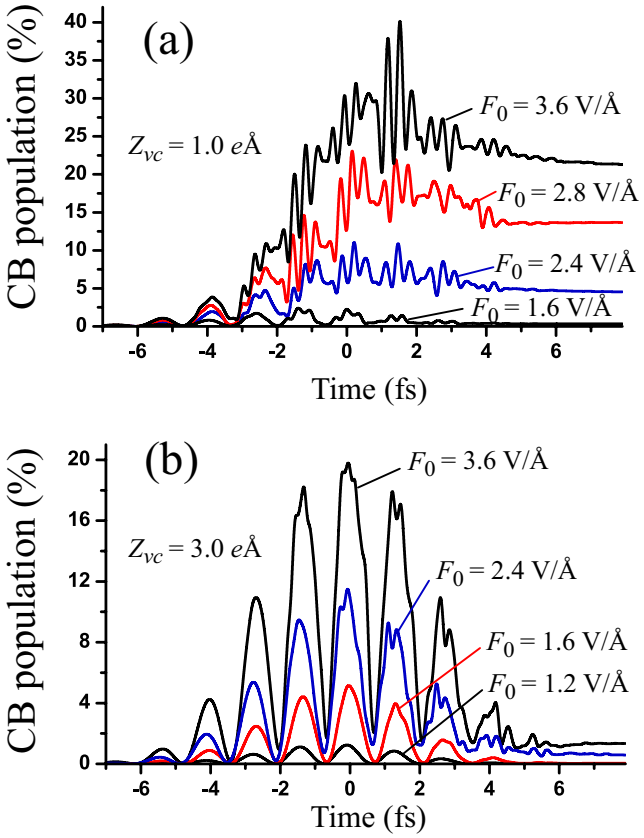

FIG. 11: Time dependent CB population is shown for different amplitudes of the laser pulse and different values of parameter Z_{vc}: (a) $Z_{vc} = 3.0$ eÅ and (b) $Z_{vc} = 1.0$ eÅ. The numbers next to the lines are the corresponding amplitudes of the laser field. The thickness of the film is 100 nm. At $Z_{vc} = 1.0$ eÅ [panel (b)] there is a large residual population of the conduction band, while at $Z_{vc} = 3.0$ eÅ [panel (a)] the residual population of the conduction band is small.

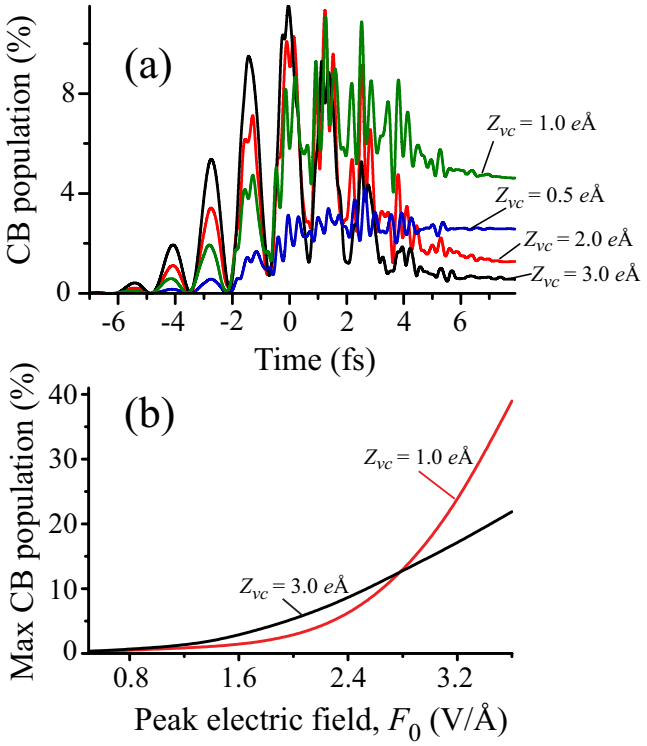

FIG. 12: Population of the CB versus time and peak electric field. The thickness of the film is 100 nm. (a) Time dependent CB population is shown for a given amplitude of the laser pulse, $F_0 = 2.4$ V/Å, and different values of parameter Z_{vc} as indicated. (b) The maximum CB population as a function of the peak electric field F_0 for two values of the interband dipole matrix element $Z_{vc} = 1.0$ eÅ (red curve) and $Z_{vc} = 3.0$ eÅ (black curve).

and Sec. V].

The dynamics of the CB population for the case of large dipolar coupling, $Z_{vc} = 3.0$ eÅ, is illustrated in Fig. 11 (b). The most dramatic feature is the sharply reduced residual population as compared to Fig. 11 (a), $\mathcal{N}_c < 2\%$ for all fields. This indicates high reversibility of the excitation in this case. The peak population is reached close to the maximum of the excitation pulse ($t = 0$); its value at the highest field is significantly reduced comparing to the case of weak coupling. Physically, this counterintuitive behavior (the reduction of the residual and maximum populations with respect to the case of weak coupling) is related to fact that the WS anticrossings occur at a higher field, and the one within the range of fields considered ($\Delta l = 2$) is highly diabatic, which prevents a large population transfer.

The dependence of the CB population $\mathcal{N}_c$ on the dipolar coupling constant Z_{vc} at a fixed pulse amplitude $F_0 = 2.4$ V/Å is displayed in Fig. 12 (a). In the initial part of the excitation pulse ($t < -1$ fs), i.e., for low excitation fields, the population $\mathcal{N}_c$ monotonously increases with Z_{vc}, as intuition would predict. At the pulse maximum, the dependence on Z_{vc} saturates but still is monotonous. In contrast, the residual ($t > 6$ fs) population dependence on the dipolar coupling is non-monotonous. For a low coupling, $Z_{vc} = 0.5 - 1$ eÅ, $\mathcal{N}_c$ increases with Z_{vc}, which is characteristic of the diabatic case where the coupling is mostly perturbative. Counterintuitively, with further increase of the coupling, $Z_{vc} > 1$ eÅ, the residual population *decreases* with increase of Z_{vc}. This is related to the fact that only the last anticrossing (the one with $\Delta l = 1$), which can have a significant anticrossing gap, shifts to larger, unattainable fields. The anticrossing gaps for $\Delta l \geq 2$ are very small and, consequently, the corresponding dynamics is deeply diabatic. This deeply diabatic dynamics is mostly perturbative and contributes little to the population transfer.

The CB population $\mathcal{N}_c$ at its maximum value during the pulse determines the heat production and damage of the dielectric. This important quantity is displayed in Fig. 12 (b) against the peak electric field for two typical values of the interband dipole element Z_{vc}. The free electron gas populating CB is characterized by the ratio

$\eta = R_{TF}/a_B$, where R_{TF} is the Thomas-Fermi screening radius and a_B is the Bohr radius,

$$R_{TF} = \frac{2e\sqrt{m_c^*}\,(3n)^{1/6}}{\pi^{1/6}\hbar\sqrt{\epsilon}}\ , \tag{42}$$

$$a_B = \frac{\epsilon\hbar^2}{m_c^* e^2}\ , \tag{43}$$

where $n = 2\mathcal{N}_c/a^3$ is the maximum CB electron density, $\epsilon \approx 2.3$ is the silica permittivity, and m_c^* is the electron effective mass for the CB, whose experimental value is[46] $m_c^* \approx 0.86m$.

The electron gas in the CB possesses metallic behavior for $\eta \lesssim 1$ which means that excitons are screened out, and the electrons behave as a free gas. Judging from Fig. 12 (b), such a behavior sets on for $F_0 \gtrsim 2.5$ V/Å (irrespectively of Z_{vc}) where $\mathcal{N}_c \gtrsim 0.15$ and, correspondingly [see Eqs. (42)-(43)], $\eta \lesssim 1.2$. Thus, $F_0 \approx 2.5$ V/Å is the breakdown field amplitude, which corresponds to the peak pulse intensity $\approx 1.7 \times 10^{14}$ W/cm^2.

V. CONCLUDING DISCUSSION

Let us briefly summarize fundamentals and main results of this article. One of the main points is nondamaging character and reversibility of the interaction of intense and ultrashort laser pulses with a dielectric. These are determined by the maximum and residual electron population, $\mathcal{N}_c$, of the CB – see Figs. 11 and 12. In these figures, we can see that the maximum CB population grows dramatically to $\sim 20-40\%$ for the peak external field $F_0 = 2.4-3.6$ V/Å corresponding to the peak intensity $\sim 1.5\times10^{14}-3.4\times10^{14}$ W/cm^2. These numbers are rather reliable because they relatively weakly depend on the interband dipole matrix element Z_{vc} whose exact value is not precisely known. As we have shown at the end of Sec. IV B, it is likely that the metallic behavior of the electron gas in the CB and, correspondingly, breakdown occur for the peak field $F_0 \gtrsim 2.5$ V/Å or peak pulse intensity $\gtrsim 1.7 \times 10^{14}$ W/cm^2.

Previously it has been predicted[25] that for significantly longer 16-fs pulses with a twice higher carrier frequency of 3.1 eV the breakdown intensity is $\approx 10^{15}$ W/cm^2. This is significantly higher than predicted by our calculations for $\approx$ 4-fs pulses of 1.55 eV frequency. This difference is even more significant if one keeps in mind that the damage threshold should considerably decrease with increasing the pulse length and carrier frequency. Notice that our coherent approach is not applicable for such long pulses as 16-fs due to importance of electron-electron scattering at such long times.

The effective reversibility of the pulse-film interaction is mostly determined by the *residual* CB population after the end of the pulse: such a low population implies that the next pulse would feel almost the same system as the initial one. One has to keep in mind that the residual CB population decays due to radiative interband transitions and lives for a very long time ~ 100 ps[47], which is many orders of magnitude longer than the characteristic times of the process of excitation and dephasing relaxation considered in our article. In contrast to the maximum CB population, the residual one very significantly depends on the interband dipole matrix element Z_{vc} – cf. Figs. 11 (a) and (b) and also see Fig. 12. Interestingly enough, the dependence on Z_{vc} is non-monotonic: it is increasing for $Z_{vc} \lesssim 1$ eÅ and sharply decreasing for $Z_{vc} \gtrsim 1$ eÅ.

This highly nontrivial dependence is due to the fact that the residual population of the conduction band is most efficiently created in the case intermediate between the pure adiabatic and diabatic regimes where the adiabatic parameter $\delta \sim 1$. In fact, in the extreme adiabatic case ($\delta \ll 1$), the population at the leading edge of the pulse is very efficiently transferred to the CB at the level anticrossing point, just as it happens in the process of the adiabatic metallization[11]. However, at the trailing edge the population transfer at the anticrossing point occurs in the reverse direction, to the VB, resulting in a very low residual CB population[13]. Such reversibility is generally characteristic of adiabatic processes. In the opposite limiting case of a very diabatic process ($\delta \gg 1$), the anticrossings are largely ignored by the system, and very little population transfer occurs. Only in the intermediate case, $\delta \sim 1$, there is a significant residual population of the CB as we have already discussed above in conjunction with Fig. 10.

A major observable quantity in our work is reflectance of the strong ultrashort pulses from the dielectric nanofilm. The predicted reflectance of a pulse increases with the pulse peak field F_0 [Fig. 5(b)] much stronger than the perturbative theory of Kerr effect suggests. This implies that the response of the nanofilm is deeply non-perturbative even in the range below the presumed breakdown threshold $F_0 \approx 2.5$ V/Å. Interestingly enough, the waveform of the reflected pulse is almost identical to that of the incident pulse. This is a consequence of the reversibility of the pulse interaction with the nanofilm under our conditions; if this interaction were not reversible, e.g., if a significant electron population were accumulated in the CB toward the end of the pulse, then the trailing edge of the reflected pulse would be significantly higher than the leading edge due to a plasma-like response.

The underlying cause of the high reflectivity is the "softening" of the dielectric, i.e., a significant increase of its polarizability, in the strong field, which is illustrated in Fig. 6. This softening is significant: the corresponding contribution to the maximum permittivity is large, $\varepsilon_{\text{eff}} = 4\pi \max\left[|\chi_{\text{eff}}|\right] \approx 2.5$, which causes more than doubling the permittivity of silica. This is related to the allowed low-frequency transitions between the adiabatic energy levels of the system in the vicinities of the anticrossings of the Wannier-Stark levels shown in Fig. 7.

The phenomena described above in this article are driven by the instantaneous pulse field rather than its intensity or field integral ("area" of the pulse). This points

toward a fundamental possibility of ultrafast (with bandwidth comparable to the optical frequency) field effect devices based on dielectrics similar to but much faster than the field effect transistors (FETs)[48–50] fabricated from the much "softer" semiconductors. To explain this analogy, in the case of the FET, the charges at the gate electrode by their electrostatic field attract the minority carriers causing the adjacent channel of the FET to conduct. Similarly, in our case the instantaneous electric field of the light wave may be thought of as inducing the appearance of the carriers (electrons in the previously empty conduction band and the respective holes in the valence band), which causes the dielectric to conduct.

To conclude, we have described a number of highly-nonlinear (non-perturbative) phenomena in dielectric (silica) nanofilms subjected to nearly-single-period strong optical pulses whose field can be just below the predicted breakdown threshold of ~ 2.5 V/Å. These results show possibility of fundamental phenomena and applications based on field control of dielectrics very much similar to the phenomena occurring in semiconductors used in field-effects transistors. The strong but short optical fields lead to the optical-electric softening of the dielectrics. These phenomena are defined by the instantaneous optical field rather then the pulse intensity or its field integral. Thus these phenomena are among the fastest in optics.

Acknowledgments

This work was supported by Grant No. DEFG02-01ER15213 from the Chemical Sciences, Biosciences and Geosciences Division and by Grant No. DE-FG02-11ER46789 from the Materials Sciences and Engineering Division of the Office of the Basic Energy Sciences, Office of Science, U.S. Department of Energy.

[1] M. Gertsvolf, M. Spanner, D. M. Rayner, and P. B. Corkum, J. Phys. B **43**, 131002 (2010).
[2] A. V. Mitrofanov, A. J. Verhoef, E. E. Serebryannikov, J. Lumeau, L. Glebov, A. M. Zheltikov, and A. Baltuška, Phys. Rev. Lett. **106**, 147401 (2011).
[3] M. Lenzner, J. Kruger, S. Sartania, Z. Cheng, C. Spielmann, G. Mourou, W. Kautek, and F. Krausz, Phys. Rev. Lett. **80**, 4076 (1998).
[4] R. H. Fowler and L. Nordheim, Proc. Royal Soc. London. Ser. A **119**, 173 (1928).
[5] C. Zener, Proc. Royal Soc. A **145**, 523 (1934).
[6] L. V. Keldysh, J. Exptl. Theor. Phys. 33, 763-770 (1957); Translation: Sov. Phys. JETP **6**, 994 (1958).
[7] G. H. Wannier, Phys. Rev. **117**, 432 (1960).
[8] M. Lenzlinger and E. H. Snow, J. Appl. Phys. **40**, 278 (1969).
[9] M. Kruger, M. Schenk, and P. Hommelhoff, Nature **475**, 78 (2011).
[10] S. Ghimire, A. D. DiChiara, E. Sistrunk, P. Agostini, L. F. DiMauro, and D. A. Reis, Nature Phys. **7**, 138 (2011).
[11] M. Durach, A. Rusina, M. F. Kling, and M. I. Stockman, Phys. Rev. Lett. **105**, 086803 (2010).
[12] L. Miaja-Avila, C. Lei, M. Aeschlimann, J. L. Gland, M. M. Murnane, H. C. Kapteyn, and G. Saathoff, Phys. Rev. Lett. **97**, 113604 (2006).
[13] M. Durach, A. Rusina, M. F. Kling, and M. I. Stockman, Phys. Rev. Lett. **107**, 086602 (2011).
[14] W. Franz, Z. Naturforschung A **13**, 484 (1958).
[15] L. Keldysh, J. Experimentl. Theor. Phys. 34, 5, 1138-1141 (1958); Translation: Sov. Phys. JETP **7**, 788 (1958).
[16] D. A. B. Miller, D. S. Chemla, T. C. Damen, A. C. Gossard, W. Wiegmann, T. H. Wood, and C. A. Burrus, Phys. Rev. Lett. **53**, 2173 (1984).
[17] D. A. B. Miller, D. S. Chemla, T. C. Damen, A. C. Gossard, W. Wiegmann, T. H. Wood, and C. A. Burrus, Phys. Rev. B **32**, 1043 (1985).
[18] I. Franco, M. Shapiro, and P. Brumer, Phys. Rev. Lett. **99**, 126802 (2007).
[19] B. C. Stuart, M. D. Feit, S. Herman, A. M. Rubenchik, B. W. Shore, and M. D. Perry, Phys. Rev. B **53**, 1749 (1996).
[20] A. Kaiser, B. Rethfeld, M. Vicanek, and G. Simon, Phys. Rev. B **61**, 11437 (2000).
[21] J. R. Peano, P. Sprangle, B. Hafizi, W. Manheimer, and A. Zigler, Phys. Rev. E **72**, 036412 (2005).
[22] L. Hallo, A. Bourgeade, V. T. Tikhonchuk, C. Mezel, and J. Breil, Phys. Rev. B **76**, 024101 (2007).
[23] B. Chimier, O. Utza, N. Sanner, M. Sentis, T. Itina, P. Lassonde, F. Lgar, F. Vidal, and J. C. Kieffer, Phys. Rev. B **84**, 094104 (2011).
[24] T. Otobe, M. Yamagiwa, J. I. Iwata, K. Yabana, T. Nakatsukasa, and G. F. Bertsch, Phys. Rev. B **77**, 165104 (2008).
[25] T. Otobe, K. Yabana, and J. I. Iwata, J. Phys.: Condens. Mat. **21**, 064224 (2009).
[26] K. Yabana, T. Sugiyama, Y. Shinohara, T. Otobe, and G. F. Bertsch, Phys. Rev. B **85**, 045134 (2012).
[27] G. H. Wannier, *Elements of Solid State Theory* (Cambridge University Press, Cambridge, England, 1959).
[28] F. Bloch, Z. Phys. A **52**, 555 (1929).
[29] K. S. Kunz and R. J. Luebbers, *The Finite Difference Time Domain Method for Electromagnetics* (CRC Press, Boca Raton, 1993).
[30] A. Taflove, *Computational Electrodynamics: The Finite-Difference Time-Domain Method* (Artech House, Boston, 2005).
[31] M. I. Stockman, Opt. Express **19**, 22029 (2011).
[32] J. C. Slater and G. F. Koster, Phys. Rev. **94**, 1498 (1954).
[33] T. Frauenheim, G. Seifert, M. Elstner, Z. Hajnal, G. Jungnickel, D. Porezag, S. Suhai, and R. Scholz, Phys Status Solidi B **217**, 41 (2000).
[34] S. Glutsch, Phys. Rev. B **69**, 235317 (2004).
[35] M. Grifoni and P. Hanggi, Phys. Rep. **304**, 229 (1998).
[36] J. Bleuse, G. Bastard, and P. Voisin, Phys. Rev. Lett. **60**, 220 (1988).
[37] E. E. Mendez, F. Agull-Rueda, and J. M. Hong, Phys. Rev. Lett. **60**, 2426 (1988).
[38] E. E. Mendez and G. Bastard, Phys. Today **46**, 34 (1993).
[39] C. Zener, Proc. Royal Soc. A **137**, 696 (1932).

[40] W. V. Houston, Phys. Rev. **57**, 184 (1940).
[41] P. M. Schneider and W. B. Fowler, Phys. Rev. Lett. **36**, 425 (1976).
[42] R. W. Ziolkowski, J. M. Arnold, and D. M. Gogny, Phys. Rev. A **52**, 3082 (1995).
[43] J. Paul, C. Christopoulos, and D. W. P. Thomas, Int. J. Numer. Model. El. **22**, 129 (2009).
[44] O. S. Heavens, *Optical Properties of Thin Solid Films* (Dover, New York, 1991).
[45] R. W. Boyd, *Nonlinear Optics* (Academic Press, London and San Diego, 2003).
[46] S. Zafar, K. A. Conrad, Q. Liu, E. A. Irene, G. Hames, R. Kuehn, and J. J. Wortman, Appl. Phys. Lett. **67**, 1031 (1995).
[47] Q. Sun, H. B. Jiang, Y. Liu, Y. H. Zhou, H. Yang, and Q. H. Gong, Chinese Phys. Lett. **23**, 189 (2006).
[48] D. Kahng, United States Patent 3,102,230 (1963).
[49] K. F. Brennan, *The Physics of Semiconductor Devices with Applications to Optoelectronic Devices* (Cambridge University Press, Cambridge and New York, 1999).
[50] S. M. Sze, *Physics of Semiconductor Devices* (Wiley-Interscience, Hoboken, N.J., 2007).